Supplementary Information

Hierarchically Structured Spherulitic Cobalt Hydroxide Carbonate as a Precursor to Ordered Nanostructures of Electrocatalytically Active Co_3O_4

Anna S. Schenk,[a,#] Miriam Goll,[a] Lukas Reith,[a] Manuel Roussel,[b] Björn Blaschkowski,[c] Sabine Rosenfeldt,[d] Xiaofei Yin,[e] Wolfgang W. Schmahl,[e] and Sabine Ludwigs*[a]*

[a] *IPOC – Functional Polymers, Institute of Polymer Chemistry, University of Stuttgart, Pfaffenwaldring 55, D-70569 Stuttgart, DE*

[b] *Institute of Materials Science, University of Stuttgart, Heisenbergstraße 3, D-70569 Stuttgart, DE*

[c] *Institute of Inorganic Chemistry, University of Stuttgart, Pfaffenwaldring 55, D-70569, Stuttgart, DE*

[d] *Department of Chemistry, University of Bayreuth, Bavarian Polymer Institute (BPI), Universitaetsstrasse 30, 95447 Bayreuth, DE*

[e] *Ludwig-Maximilians-Universitaet Munich, Department fuer Geo- und Umweltwissenschaften, Sektion Kristallographie, Theresienstrasse 41, 80333 Munich, DE*

 # Present address: Physical Chemistry – Colloidal Systems, Bavarian Polymer Institute (BPI), University of Bayreuth, Universitaetsstrasse 30, 95447 Bayreuth, DE

**E-mail: anna.schenk@uni-bayreuth.de and sabine.ludwigs@ipoc.uni-stuttgart.de*

Contents

1. Experimental Details on the Characterization of Precursor Materials and Oxides

A range of imaging, spectroscopic and x-ray scattering techniques were applied to study the chemical composition and structure of the precipitates before and after annealing.

(Polarized) light optical microscopy. The overall morphology of the particles before and after annealing was examined by light microscopy using a VHX-950F digital microscopy system from Keyence. Polarized light microscopy was performed to study the crystallinity of the materials using an Axio Imager A1m microscope from Zeiss equipped with an AxioCam 1Cc1 camera.

Scanning Electron Microscopy. The samples were fixed on SEM stubs with the help of adhesive carbon tapes and examined in their pristine state without an additional conductive coating. Images were recorded using a Hitachi S-4800 instrument operated in the deceleration mode with a landing voltage of 0.5 or 1 kV.

Transmission Electron Microscopy. TEM and selected area electron diffraction (SAED) of precursor precipitates as well as cobalt(II,III) oxide samples obtained after calcination were performed on a Phillips CM-200 FEG-TEM operating at 200 kV. Samples containing microparticles were slightly ground with a mortar and pestle. The resulting powders were then dispersed in ethanol and a small droplet of these suspensions was pipetted onto copper TEM grids coated with a film of Formvar and carbon. The samples were dried under vacuum before being transferred to the electron microscope.

Infra-red Spectroscopy. Vibrational spectra of powdered samples were measured using an IFS 66/S FT-IR spectrometer from Bruker covering a wavelength range from 700-3500 cm^{-1}. The instrument was equipped with a diamond ATR (golden gate) unit purchased from Specac.

Thermogravimetric Analysis (TGA) and Differential Scanning Calorimetry (DSC). The composition of the precursor phase and the transformation into cobalt(II,III) oxide was investigated by TGA and DSC using an STA 449C instrument (NETZSCH, Germany). Data were recorded under synthetic air atmosphere (100 $mL \cdot min^{-1}$) in a temperature range of 25°C-600°C with a heating rate of $10°C \cdot min^{-1}$.

Powder X-ray Diffraction. X-ray diffraction of finely ground powders was performed to identify the mineral phases present in the samples and to study their crystallinity. Initial measurements were performed with Cu-$K\alpha_1$ radiation in Bragg-Brentano geometry on an XRD 3003 TT diffractometer (GE Sensing & Inspection Technologies, Hürth, Germany) at 40 kV and 30 mA. Data were recorded in an angular range between 10° and 120° in steps of 0.013° with a total exposure time of 800 s.

Alternatively, with the aim to reduce the background due to X-ray fluorescence, diffractograms were also obtained using a STOE STADI P system equipped with a molybdenum source (λ = 0.7107 Å) and a

Mythen 1K-PSD detector. The calculation of lattice parameters was performed with the software package Treor.[1]

Small-angle X-ray scattering. SAXS data of powdered samples filled into glass capillaries (∅ = 1 mm, Hilgenberg) were recorded using a Double Ganesha AIR system (SAXSLAB, Denmark). Monochromatic radiation with a wavelength of λ = 0.154 nm was provided by a rotating anode (MicroMax 007HF, Rigaku Corporation, Japan). Two-dimensional scattering patterns were collected with a position-sensitive detector (PILATUS 300 K, Dectris), which was placed at different distances from the sample to cover a range of scattering vectors q between 0.1 and 6 nm^{-1}. The radially averaged profiles of the scattering intensity versus the modulus of the scattering vector **q** ($|\boldsymbol{q}| = q = \frac{4\pi\sin(\theta)}{\lambda}$, where 2θ is the scattering angle and λ represents the wavelength of the incident beam) were corrected for instrument-related background, sample thickness and scattering attributable to the sample container and subsequently merged. Sample-related background including angle-independent Laue scattering as well the possible contribution of a homogeneous fluorescence signal were removed by modelling the intensity at large q by a power law $I(q) \sim q^{-a} + c$ and subtracting the constant c from the data.

UV-Vis Absorption Spectroscopy. A Lambda 35 UV/Vis spectrometer from Perkin Elmer (Rodgau, Germany) was used to record characteristic absorption spectra of solutions containing either pure $CoCl_2$ ($[Co^{2+}]$ = 10 mM) or a mixture of $CoCl_2$ and the water-soluble polymer additive polyethylenimine ([PEI] = 0.1 g L^{-1}). Ultra-pure water (ELGA Maxima, resistivity of 18.2 MΩ·cm) was measured as a reference.

Electrochemical Characterization by Cyclic Voltammetry. All electrochemical experiments were performed with an Autolab PGSTAT101 potentiostat in a three-electrode glass cell in 0.1 M NaOH (ABCR GmbH) in ultrapure water (18.2 MΩcm) under inert gas atmosphere at room temperature. Cobalt hydroxide carbonate and Cobalt(II,III) oxide spherulites were immobilized on glassy carbon working electrodes. For this purpose, suspensions of the spherulites were prepared in a water/alcohol mixture together with Nafion (Nafion® 1100 EW, 5 wt.-% in a mixture of water and aliphatic alcohols, Sigma Aldrich) as binder and glassy carbon powder as conductive support. These suspensions were homogenized by ultrasonification and then drop-casted on a polished glassy carbon disc electrode with a diameter of 3 mm. The electrodes were then blown dry with argon resulting in a typical loading of 0.25 mg/cm^2 spherulites, 0.05 mg/cm^2 glassy carbon powder and 0.05 mg/cm^2 Nafion (cf. Fig. 5). A glassy carbon rod was used as counter electrode and the reference was a double junction Ag/AgCl (3M KCl) electrode with a ground-joint diaphragm. The rotation speed of the rotating disc electrode (RDE) was set to 2000 r.p.m..

Cyclic voltammograms were collected at a scan rate of 20 mV/s in a potential window of -0.3-0.6 V, to fully cover the expected positions of the redox signals attributed to the transitions $Co^{2+} \rightarrow Co^{3+}$ and $Co^{3+} \rightarrow Co^{4+}$.[2-3] In order to analyze the electrocatalytic activity of the Co_3O_4 spherulites towards the oxygen evolution reaction (OER), cyclic voltammograms were recorded in a potential window, where water splitting is enabled, at a scan rate of 10 mV/s. Overpotentials for the OER are given as $\eta = E_{RHE} - E_{H_2O/O_2}$, where E_{H_2O/O_2} is the standard potential of the OER vs the reversible hydrogen electrode (RHE, E_{H_2O/O_2} = 1.229 V) and the current density η was calculated on the basis of the geometric surface area of the electrode. The uncompensated solution resistance R_u was determined using the current-interrupt method (a typical value was 80 Ω). The measured potentials were converted to the reversible hydrogen electrode (RHE) scale and corrected for the iR-drop according to the equation $E_{RHE} = E_{Ag/AgCl} + 0.059 \cdot pH + E^0_{Ag/AgCl}$ (3M KCl) - $i \cdot R_u$, where E_{RHE} is the converted potential, $E_{Ag/AgCl}$ is the measured potential vs. the Ag/AgCl electrode, $E^0_{Ag/AgCl}$ (3M KCl) equals 0.205 V and i represents the measured current[4]. A commercial standard of Co_3O_4 (nanopowder < 50 nm particle size, Sigma Aldrich) was analyzed for comparison. Overpotentials were determined as an average obtained from at least 8 electrodes prepared according to identical protocols.

2. Supplementary Figures and Analyses

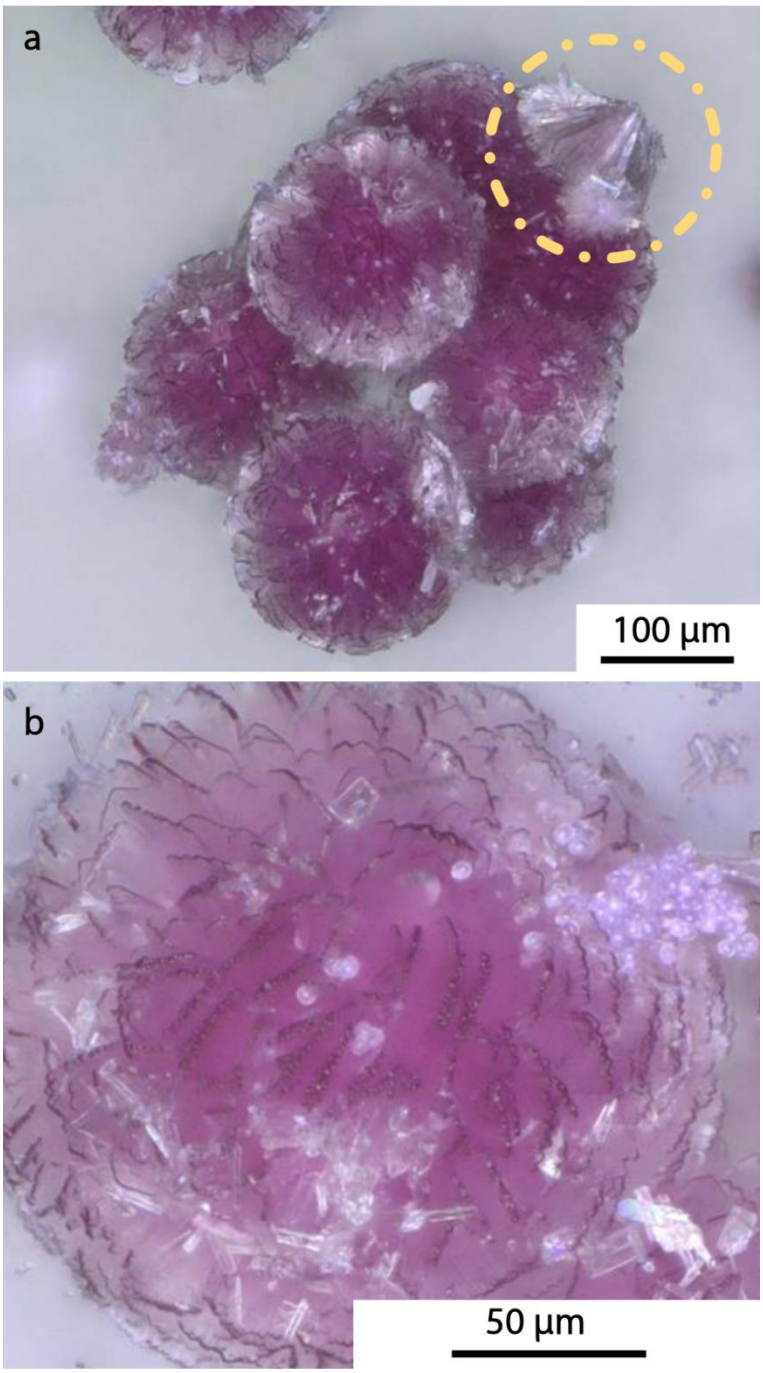

Figure S1. Light microscopy images of the precursor material obtained after aging in solution for a period of 14 days. Dark pink spherical particles, partially intergrown with each other are seen (a). A growth pattern based on platelets radially branching outwards from the particle centre is commonly observed in fracture pieces as exemplified in the encircled area in (a). An image of an individual sphere was recorded at higher magnification and shows the platelet structure in higher detail.

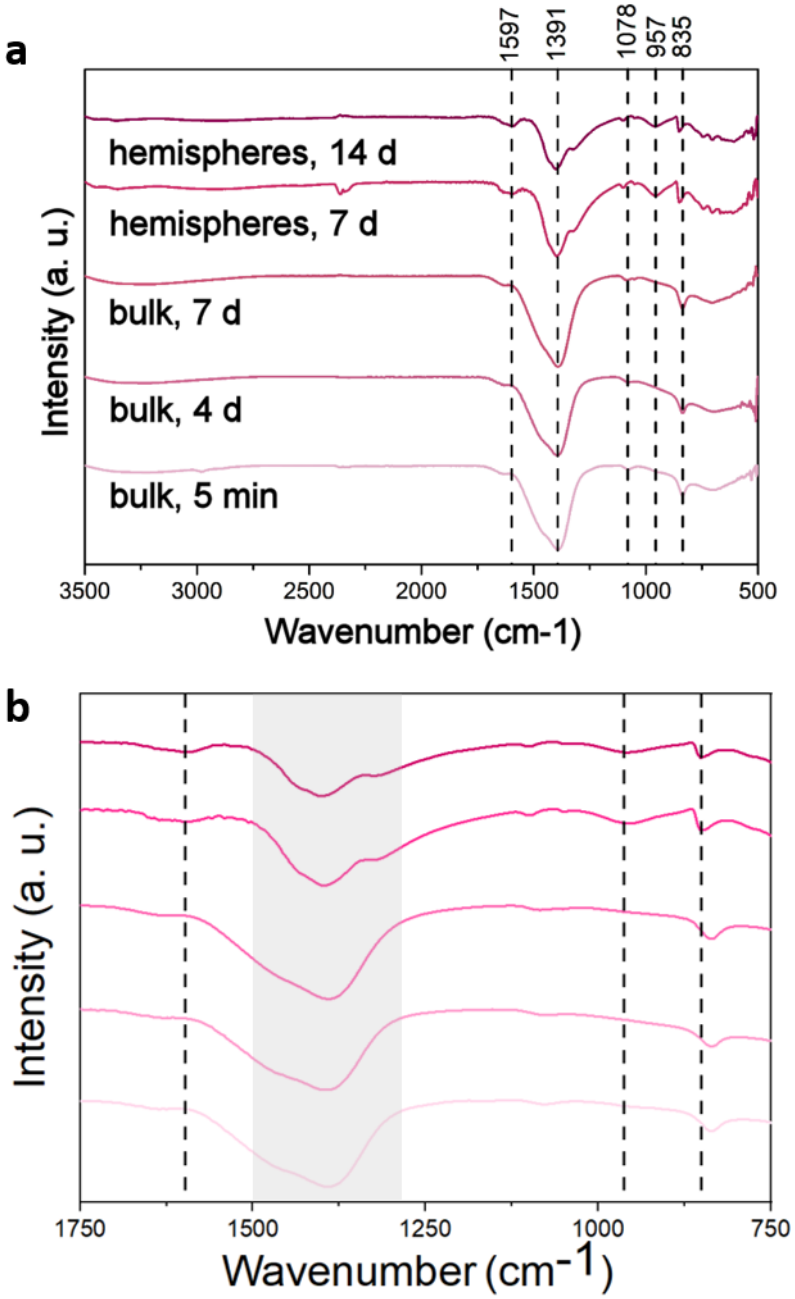

Figure S2. Infrared spectroscopy of precursor material after different reaction times. a) Full spectrum. Both, the initially deposited pale pink voluminous bulk precipitate and the platelet-based spherulitic particles formed upon recrystallization were characterized by IR spectroscopy after different periods of aging in solution. All samples showed vibration bands attributable to the presence of hydroxyl and carbonate-counterions. Specifically, characteristic signals originating from carbonate ligands were observed at 835 cm^{-1} ($\nu_2(CO_3^{2-})$), 1078 cm^{-1} ($\nu_1(CO_3^{2-})$, presumably IR-active due to symmetry reduction), and 1391 cm^{-1} ($\nu_3(CO_3^{2-})$), while the bands recorded at 957 cm^{-1} and 1597 cm^{-1} can be attributed to Co-OH and HOH deformation modes.[5]

b) A zoomed view of the spectral region between 750 - 1750 cm^{-1} is shown. When comparing the spectra, it is notable that the vibration band at 957 cm^{-1}, which can be assigned to the δ(Co-OH) bending mode, is more prominent in the mature spherulites as compared to the voluminous bulk material extracted prior to transformation. This observation is in agreement with either an increase in the proportion of hydroxyl ligands or a higher degree of order (crystallinity) in the spherulitic material.

Moreover, the $\nu_2(CO_3^{2-})$ band is shifted to higher frequencies in the hemispheres as compared to the early stage bulk precipitate, while the HOH deformation mode appears at lower wavenumbers in the mature material. This points to a distortion of bond lengths and angles within the carbonate ions and water molecules due to the interaction with mineral surfaces. In the region between 1300 and 1500 cm^{-1} (grey bar), the band corresponding to the $\nu_3(CO_3^{2-})$ vibration appears substantially broader in the initial precipitate than in the mature spherulites. As band broadening in IR spectroscopy is associated with a wider distribution of force constants of the involved bonds, and thus different chemical environments for the carbonate ions, this observation indicates a lower degree of structural order in the bulk precipitate, which then increases upon aging, where this is in agreement with a higher crystallinity of the mature spherulites.

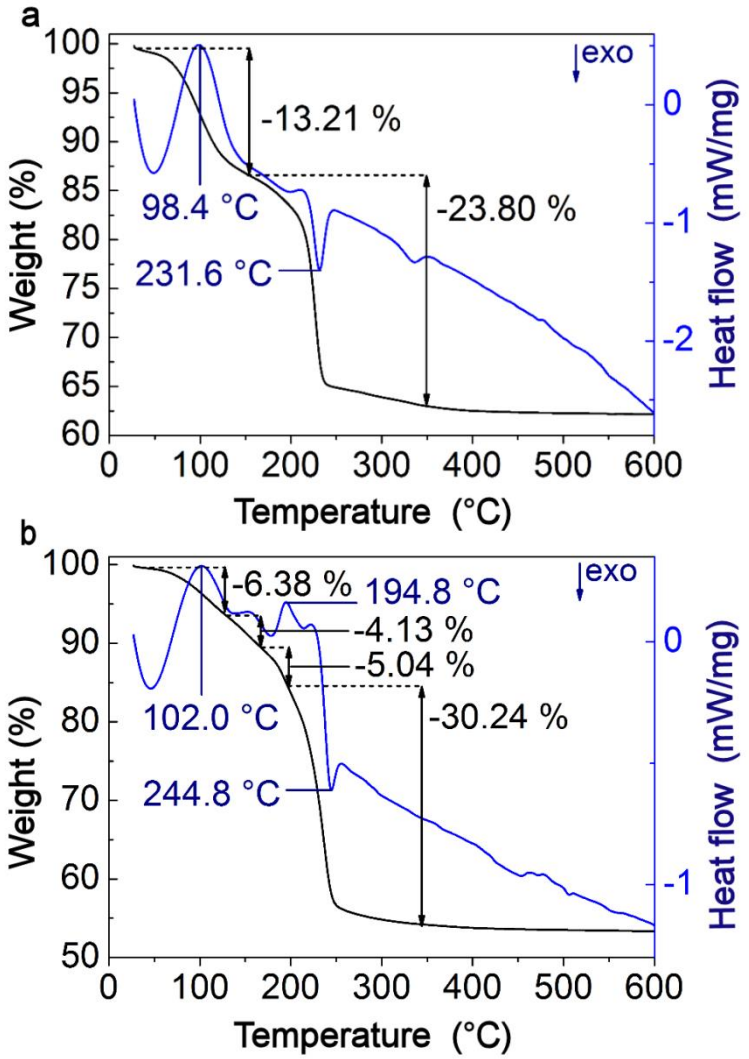

Figure S3. Thermogravimetric analysis and differential scanning calorimetry of the cobalt hydroxide carbonate precursor aged for different periods of time. The thermal decomposition and transformation of cobalt hydroxide carbonate extracted directly after mixing the reactant solutions (a) and fully-grown spherulites isolated after 14 days (b) was monitored by thermogravimetric analysis (black curves) and differential scanning calorimetry (blue curves). At temperatures in the range between 90° and 200°C a gradual mass loss was observed in both samples, which can be attributed to the elimination of surface-bound and structural water.

Differential scanning calorimetry further revealed exothermal events at 231.6°C and 244.8°C, respectively for the initial voluminous bulk precipitate and the spherulitic material obtained after aging in solution. These sharp and distinct peaks were accompanied by a substantial weight loss of the materials indicating the transformation of cobalt hydroxide carbonate into Co_3O_4 under elimination of gaseous CO_2 and H_2O.[6] A shift of the decomposition temperature to higher values can be interpreted as a higher crystallinity of the spherulites as compared to the original precipitate. Based on the assumption that the initial mass loss event at temperatures below 200°C is fully explained by the

release of water molecules, it can be calculated that the water-free initial voluminous precipitate has lost 27.4 % of its mass during the transformation into cobalt oxide, while the mass of the water-free spherulitic material is reduced by 35 %. The theoretical values for the mass loss expected during the decomposition of stoichiometric $Co(OH)_2$ and $CoCO_3$, are calculated as 13.6 % and 32.5 %, respectively according to equations (1) and (2). Based on their infrared spectra, both the initial solid and the spherulites are assumed to exhibit a general composition $Co(OH)_x(CO_3)_y$.

(1) $6\ Co(OH)_2\ (s) \xrightarrow{\Delta T, O_2} 2Co_3O_4\ (s) + 6H_2O\ (g)$

(2) $3\ CoCO_3\ (s) \xrightarrow{\Delta T, O_2} Co_3O_4\ (s) + 3CO_2\ (g)$

As the mass loss recorded for the spherulitic material is higher than the value estimated for a pure Co(II) carbonate, it can be assumed that the cobalt ions in this compound are partially oxidized to Co(III), which is in agreement with a layered double hydroxide structure based on the stacking of layers constituted by metal hydroxide octahedra with a positive net charge ($[Co^{2+}_{1-x}Co^{3+}_x(OH)_2]^{x+}$) and carbonate (as well as possibly traces of other ions) intercalated in the interlayer domain.[7-8]

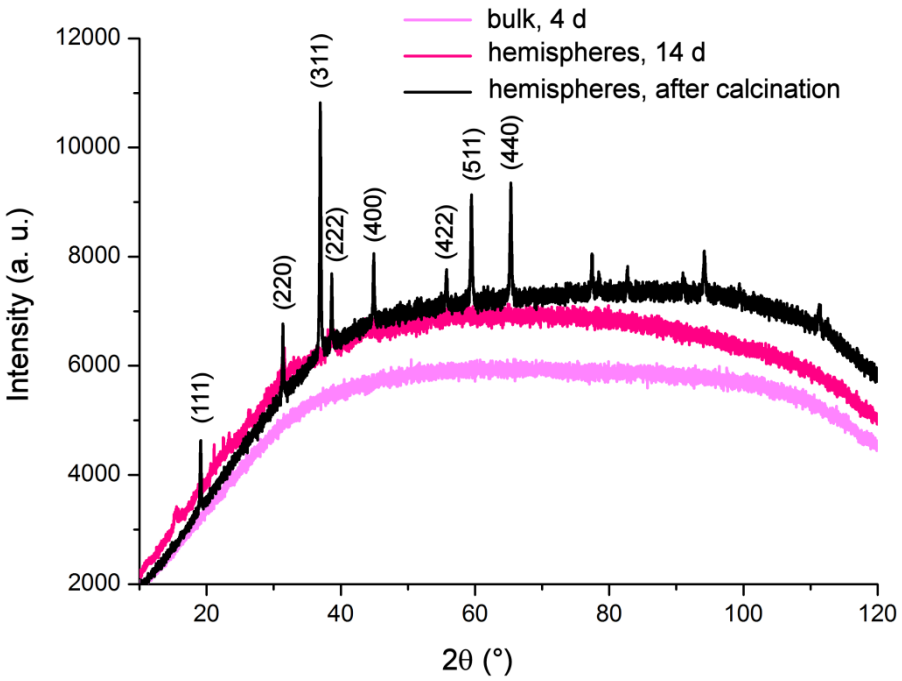

Figure S4. XRD analysis of precursor material and calcination product. Powder X-ray diffractograms comparing the voluminous bulk precipitate extracted after 4 days (light pink curve) and fully–grown spherulites before (pink curve) and after calcination (black curve) generally showed a strong background signal when recorded with Cu-Kα_1 radiation due to X-ray fluorescence. The curves obtained from the precursor materials did not exhibit discernible Bragg peaks and hence phase identification could not be performed on the basis of these data. After calcination at 400°C, in contrast, the diffractogram of the powdered material showed clearly defined Bragg peaks characteristic of Co_3O_4 (black curve). Specifically, the (111), (220), (311), (400), (422), (511), and (440) reflections of spinel-type cobalt(II,III) oxide were identified by comparison with reference data (ICDD PDF# 74-1657).[9-10] As the fluorescence background signal complicates data analysis and may even lead to incorrect phase identification, a molybdenum source was used for further experiments investigating the effects of Mn(II) and Ni(II) doping on the crystal structure.

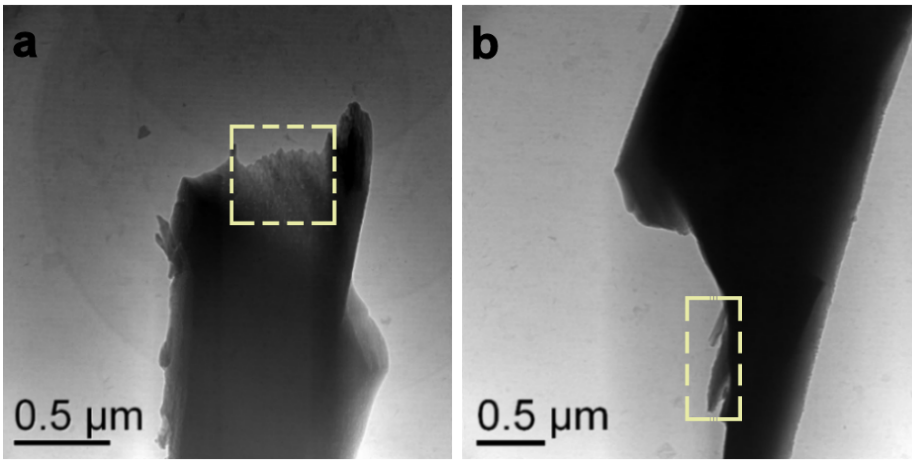

Figure S5. Transmission electron microscopy of cobalt hydroxide carbonate sheets. The platelets were isolated from spherulitic mineral particles grown from a reactant solution with concentrations of $[CoCl_2 \cdot 6H_2O] = [(NH_4)_2CO_3] = 100$ mM. Upon mechanical fracture, delamination into thinner, electron-transparent sheets is observed at the edges of the compact platelets (yellow boxes). These sheets are extremely sensitive to the electron beam and do not give a distinct signal in electron diffraction.

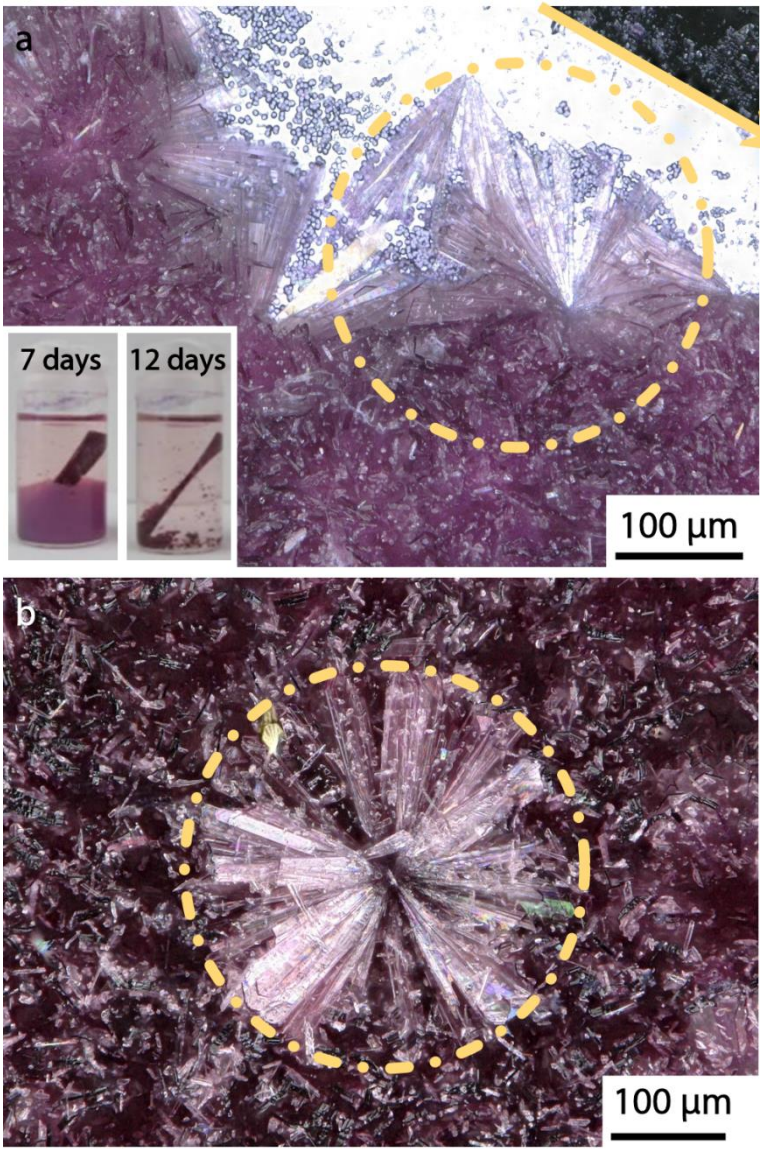

Figure S6. Cobalt hydroxide carbonate platelets deposited on SiO_x substrates. a) Complete coverage with a dark pink precipitate was observed on an SiO_x substrate placed upright into the reactant solution by light microscopy after an aging period of 12 days. Flat structures with radial symmetry (encircled area) are seen close to the edge of the substrate (yellow line). Photographs of the reaction vial taken after 7 days and 12 days, respectively indicate that the secondary nucleation of the platelet-based dark-pink material preferentially occurs on the substrate introduced into the solution and only a minor amount of (hemi-)spherical particles is formed at the glass wall. In addition, heterogeneous nucleation of the secondary phase on the SiO_x shard promotes the precursor transformation process in that the initially deposited voluminous precipitate is fully consumed after 12 days. b) While the majority of the dark-pink plate-like crystallites appear to be oriented roughly perpendicular to the substrate surface, occasionally, flat spherulitic structures composed of platelets with an orientation parallel to the substrate surface are observed (encircled area).

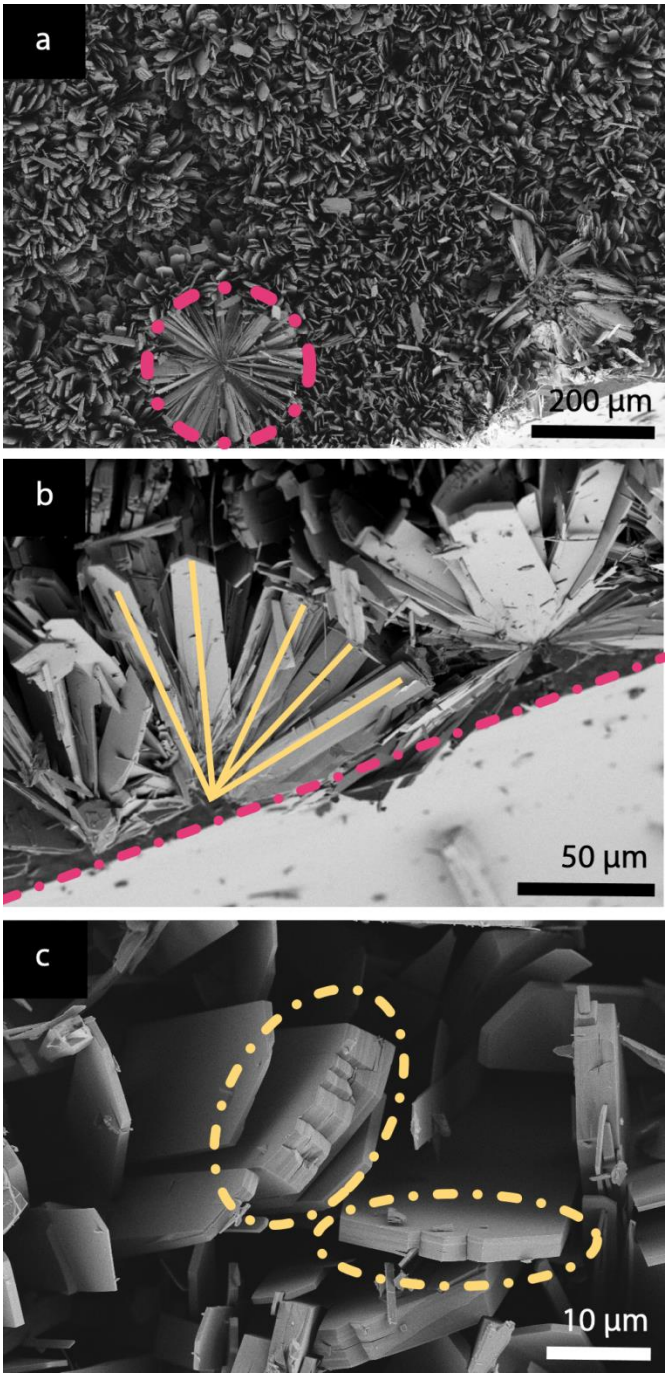

Figure S7. Scanning electron micrographs of platelet-based cobalt hydroxide carbonate structures on SiO_x substrates. A top view of the mineral-coated substrate reveals a rough-textured surface topography composed of mineral platelets largely oriented along the surface normal of the wafer. A minor fraction of flat spherulitic particles with their platelet long axes lying roughly within the substrate plane are observed (encircled area). b) Elongated mineral platelets arranged into spherulitic structures with their long axes pointing out of the substrate plane (orientation indicated by yellow lines) are seen at the edge of the SiO_x wafer shard (indicated by the pink line). c) A higher magnification image recorded from the top reveals a platelet thickness ranging from ~1 µm to 5 µm and confirms the layered substructure of the thicker plates (encircled areas).

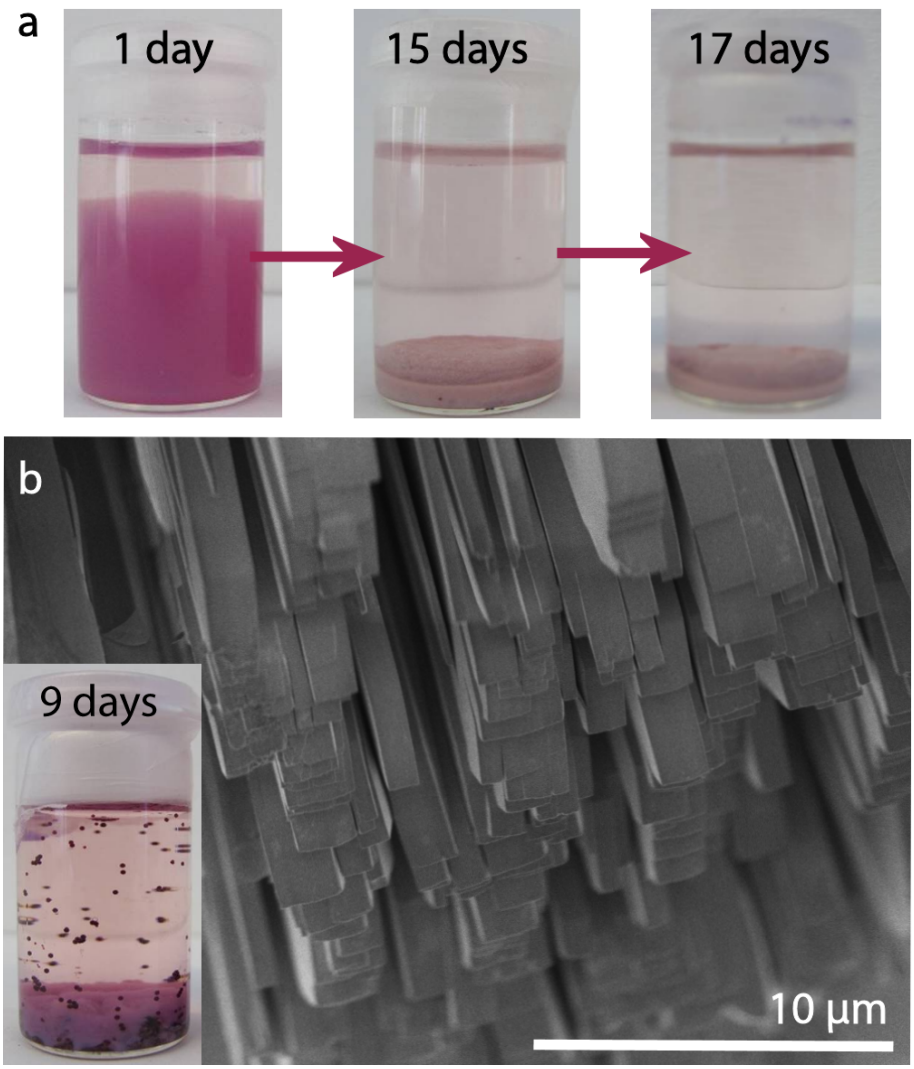

Figure S8. Variation of the reactant concentration. The effects of the initial concentration of Co(II) and ammonium carbonate on the transformation of the precursor material were investigated by depositing cobalt hydroxide carbonate from solutions of a) [$CoCl_2 \cdot 6H_2O$] = [$(NH_4)_2CO_3$] = 50 mM and b) [$CoCl_2 \cdot 6H_2O$] = [$(NH_4)_2CO_3$] = 200 mM. At lower reactant concentrations the initially deposited voluminous bulk precipitate was observed to sediment and densify over a timeframe of approximately 17 days (a). However, transformation into spherulites - as had been seen for 100 mM solutions of Co(II) and ammonium carbonate - did not occur even when the precipitate was monitored for up to 60 days. In contrast, precipitation from a highly concentrated reactant solution rapidly let to a formation of large spherulites with up to 2 mm diameter constituted from well-defined bulky mineral platelets as observed by SEM after 9 days of reaction time (b). The inset presents a photograph of the reaction vial (∅ = 1.5 cm) showing mm-sized, dark pink spherical objects at walls and the bottom of the glass container and only a minor residue of the unconsumed pale pink bulk precipitate.

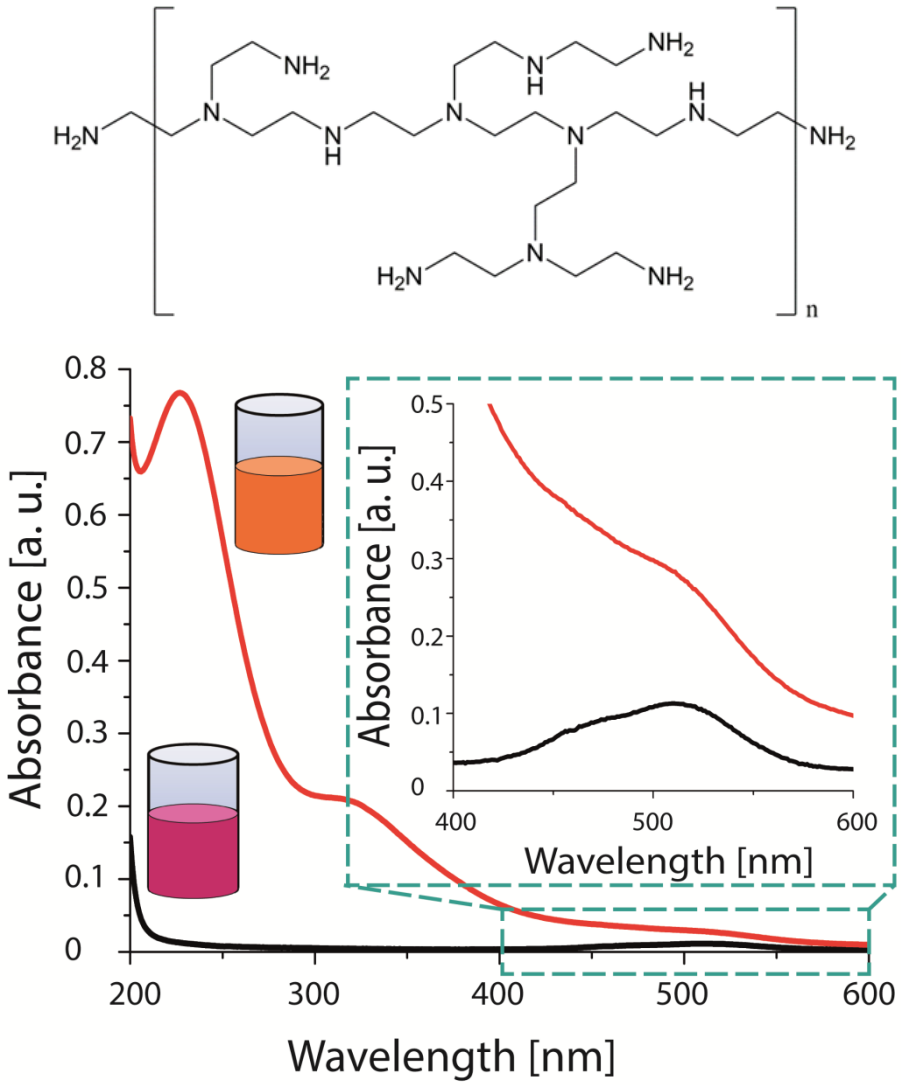

Figure S9. UV/Vis absorption spectra of a 10 mM aqueous solution of $CoCl_2$ in the absence and presence of 0.1 g L^{-1} polyethylenimine (PEI). The polymer-free Co(II)-solution (black curve) appears pink and shows a broad absorption signal with a maximum at ~520 nm (highlighted in the inset) in agreement with literature data[11]. Upon addition of the amine-functionalized polymer the color of the solution changes to orange-brown and two additional absorption bands are detected at ~225 nm and ~325 nm (red curve), thus indicating a complexation of the metal cations by the polyelectrolyte. In the absence of metal ions, PEI itself does not exhibit absorption bands in the wavelength range between 300 nm and 600 nm.[12] In the upper panel, the chemical structure of branched PEI is shown.

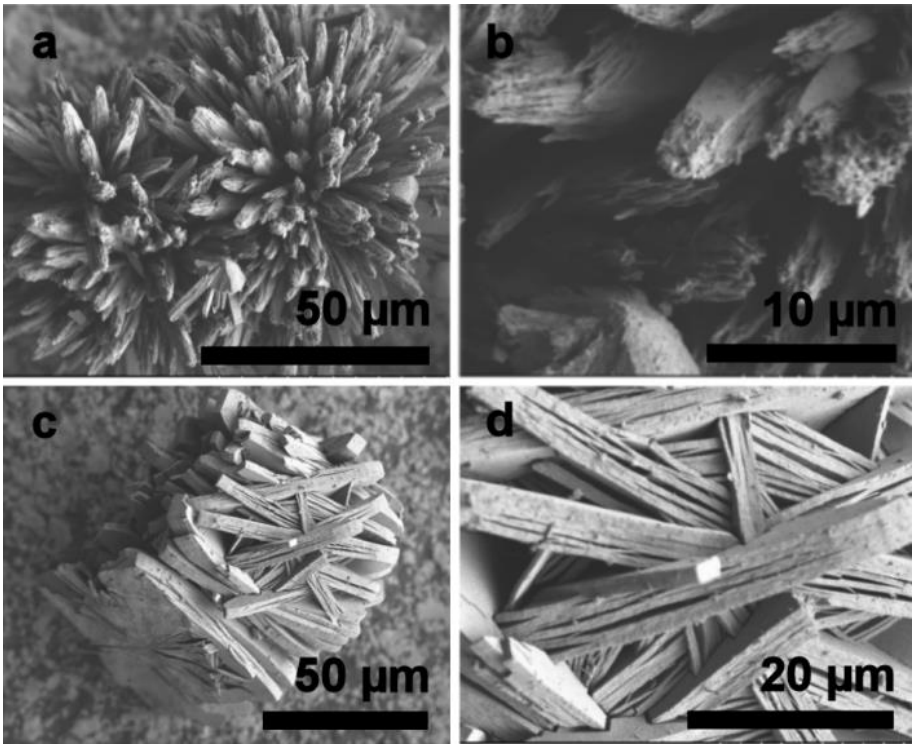

Figure S10. Effects of polyethylenimine as a structure-directing additive. Scanning electron micrographs of Co_3O_4 particles obtained by calcination of basic cobalt carbonate precipitated from a 100 mM $CoCl_2$ solution in the presence of 1 g L^{-1} PEI. The mineral precursor was removed from the solution after 15 days and annealed in air atmosphere for 2 hours at 400°C. (a, b) Spherulitic particles with frayed edges. (c, d) Aggregated platelet-based structures partially delaminated along planes parallel to the~5 µm-thick plates, thus indicating a layered substructure.

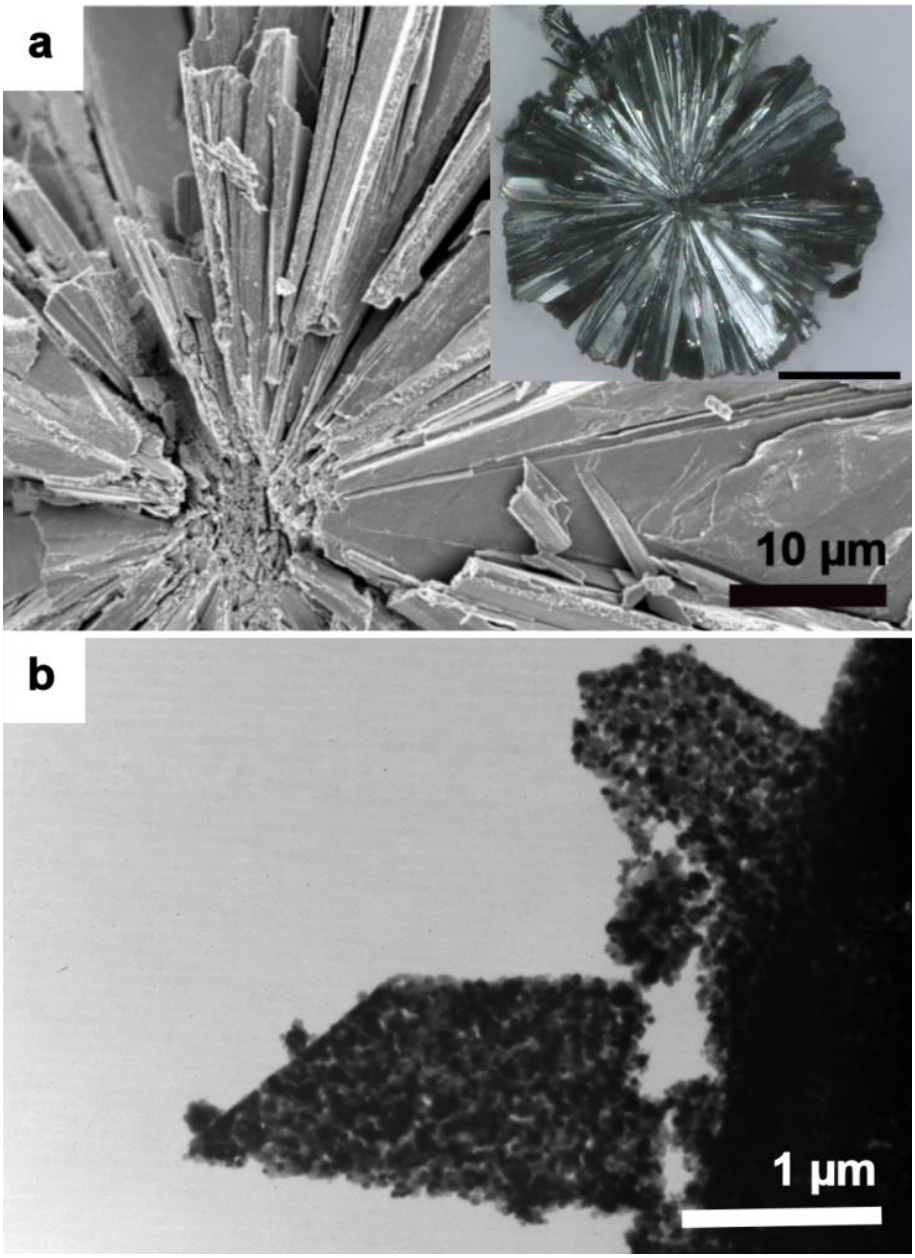

Figure S11. Morphology of the calcination product. a) Scanning electron microscopy of a Co_3O_4 particle obtained by calcination of a precursor spherulite is presented. The mineral precursor had been removed from a reactant solution with initial concentrations of $[CoCl_2{\cdot}6H_2O]$ = $[(NH_4)_2CO_3]$ = 100 mM after 14 days followed by annealing for 2 hours at 400°C in air atmosphere. Co_3O_4 platelets radiating out from the center of the spherulite, and thus resembling the structure of the precursor, are observed. Light microscopy reveals that the transformation of the basic carbonate precursor into the black spinel cobalt oxide phase, is pseudomorphic, in that the spherulitic morphology is fully retained (Inset, scale bar = 100 µm). b) A substructure constituted from interconnected nanoparticles (~ 20-50 nm) interspersed by pores with a size of ~10 nm is seen in delaminated platelets by transmission electron microscopy.

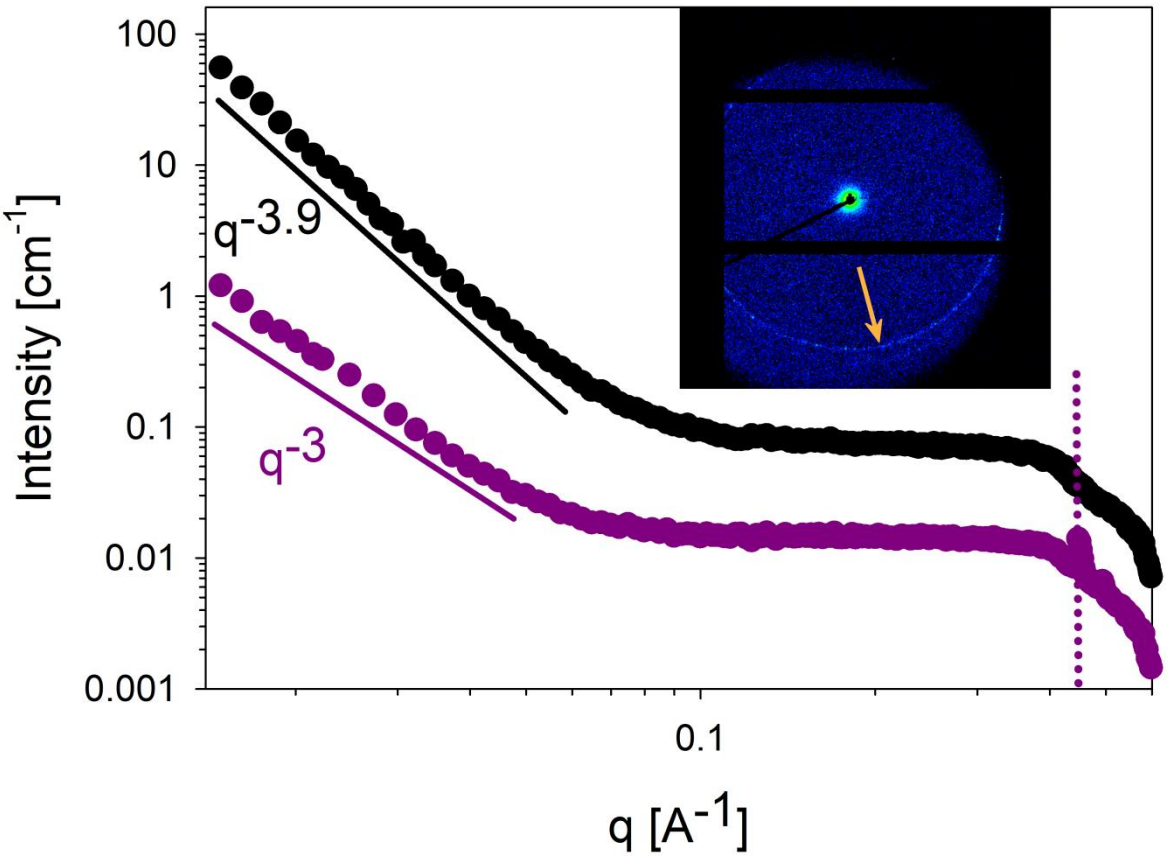

Figure S12. Small-angle X-ray scattering curves (*I(q)* vs. *q*) of $Co(OH)_x(CO_3)_y$ and Co_3O_4 spherulites. The nanostructure of spherulitic particles obtained from a reactant solution with concentrations of $[CoCl_2 \cdot 6H_2O]$ = $[(NH_4)_2CO_3]$ = 100 mM after aging the initial precipitate in solution for 14 days was investigated by small-angle X-ray scattering (pink curve, log-log representation). The prominent Bragg peak at q = 0.4478 $Å^{-1}$ (pink vertical dotted line) indicates long range periodicity in the structure and corresponds to a d-spacing of d = 14 Å. The scattering profile of the calcined sample (black curve) shows a steeper intensity decay at low q, which is in agreement with more clearly defined interfaces developing upon transformation of the basic carbonate spherulites into Co_3O_4. Inset: Two-dimensional detector image of the precursor sample (position of the Bragg reflection indicated by yellow arrow).

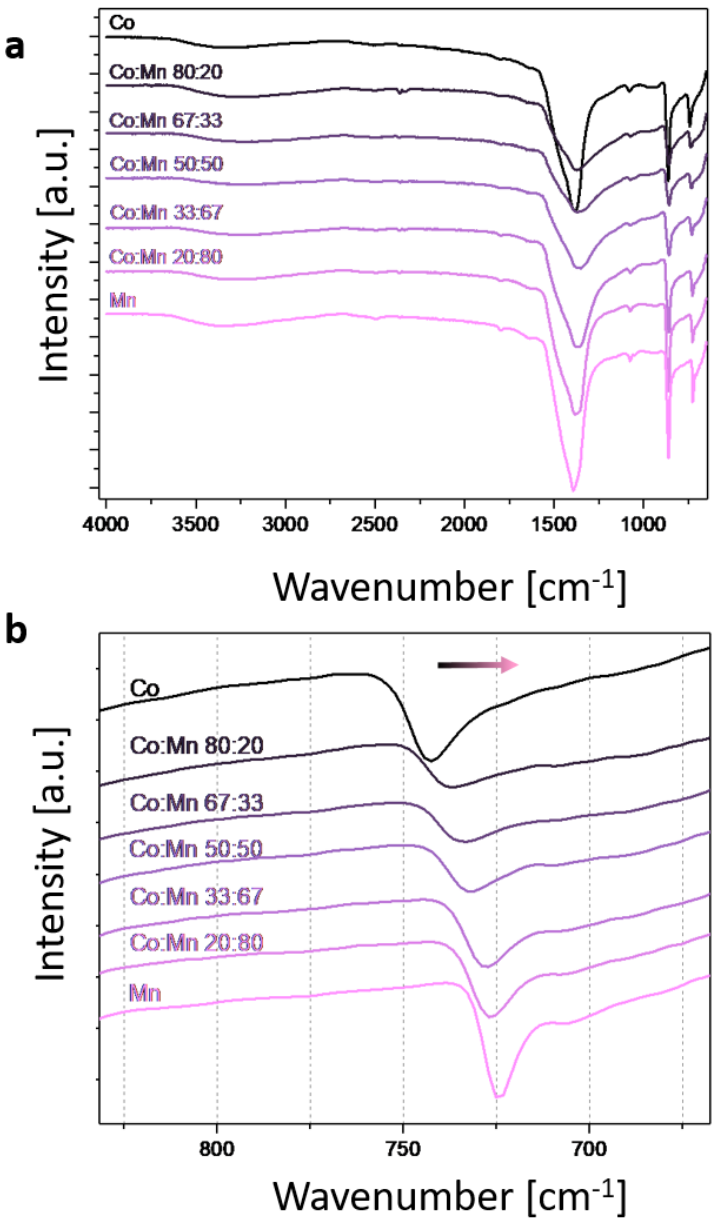

Figure S13. Infra-red spectra of mixed metal carbonates prepared by salt metathesis at different Co:Mn ratios ([(Co/Mn)Cl_2] = 100 mM, [$(NH_4)_2CO_3$] = 100 mM, aging time 7 days). A commercial $CoCO_3$ powder was measured for comparison (black line, Alpha Aesar). The vibration bands in the overview spectra (a) can be assigned to metal carbonates with calcite structure.[13] b) A detailed view of the $\nu 4$ band, which is attributed to the in-plane bending mode of the carbonate ion, reveals a systematic shift to lower wavenumbers at increasing manganese content (arrow). This observation can be explained by a gradual increase in the C-O bond length by interaction with counterions of lower mass and higher ionic radius.[14]

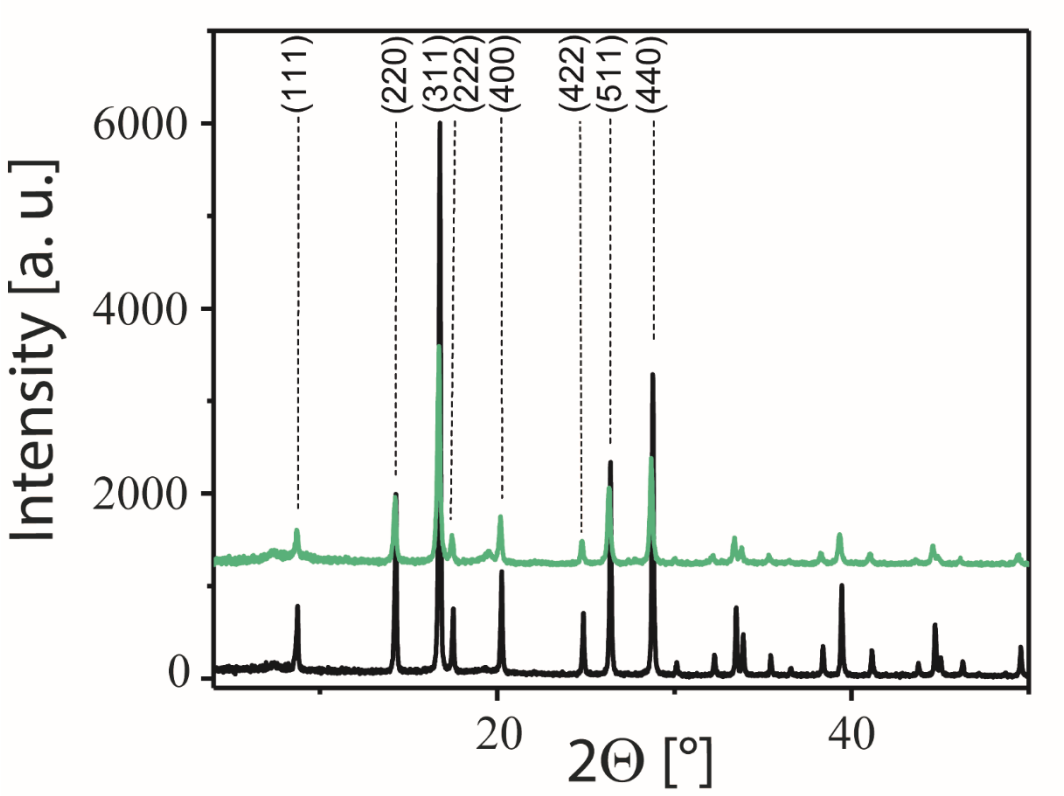

Figure S14. X-ray diffractograms comparing powders of spherulitic particles obtained by precipitation from solutions containing either $[Co^{2+}]$ = 100 mM (black line) or $[Co^{2+}]$ = 80 mM and $[Ni^{2+}]$ = 20 mM (green line) followed by aging in solution and calcination (2h, 400°C). The Bragg peaks are assigned to the cubic spinel structure (ICDD PDF# 20-781).

3. Inhibitory Effect of the Chelating Polyelectrolyte Polyethylenimine on Precursor Mineralization

With the aim to explore strategies to gain further control over the structural evolution of the cobalt-containing precursor, we investigated the influence of polyethylenimine (PEI) as a structure-directing additive. This water-soluble polyelectrolyte exhibits a branched architecture comprising primary, secondary and tertiary amine groups (Fig. S9) and is well-known to coordinate metal ions.[15] In previous works on polymer-mediated calcium carbonate precipitation the presence of PEI has been demonstrated to induce a partial polymorph switch from calcite, which is the thermodynamically most stable modification under additive-free conditions, to vaterite, a metastable polymorph, thus profoundly interfering with the crystallization process of the inorganic phase.[16] In our here investigated Co(II)-based precipitation system, the initially observed intensely pink metal-ion solution instantaneously changed its color to orange upon addition of the amine-functionalized polymer. This effect is reflected in the emergence of a characteristic absorption band at 325 nm in the UV/Vis-spectrum of a solution containing 10 mM $CoCl_2$ and 0.1 g L^{-1} PEI (Fig. S9, red curve). The absorption profile of a polymer-free $CoCl_2$ solution, in contrast, showed only one broad absorption signal centered at around 520 nm. This profound change in the absorption characteristics can be attributed to the well-documented complexation of cobalt ions by amine functional groups,[17] thus demonstrating significant interaction between the metal ions and the polymer in aqueous solution. Considering that the pK_a value of branched PEI is the range between 8.5-9.2[18] and the pH of a reaction mixture containing [$CoCl_2$] = 100 mM, [$(NH_4)_2CO_3$] = 100 mM and [PEI] = 1 g L^{-1} immediately after mixing the components is around pH = 7.5, most of the amine groups on the polymer are expected to be present in their protonated form during mineral precipitation. Therefore, electrostatic attraction between ($–NR_3^+$)-polycations and negatively charged carbonate ions has to be regarded as another important interaction mode between the polymer additive and the ions of the crystallization solution.

In our experiments on polymer-mediated precipitation of basic cobalt carbonate, PEI appeared to stabilize the initially deposited voluminous bulk precipitate, in that sedimentation of the solid and secondary nucleation were significantly delayed in the presence of the polyelectrolyte. Indeed, even after increasing the aging period to 60 days, transformation of the original light pink bulk precipitate into compact spherulitic structures was still not found to be completed. Moreover, the fraction of basic cobalt carbonate that did eventually undergo structural reorganization, comprised particles significantly smaller and less regular in shape than those obtained under additive-free conditions (Fig. S10). Concomitantly, the surface features on some of the resulting crystals were conspicuously finer and even appeared fringed and fibrous. It is interesting to note that upon drying we often observed delamination of the platelets along their surface normal.

Supporting References

1. Werner, P.-E.; Eriksson, L.; Westdahl, M., TREOR, a semi-exhaustive trial-and-error powder indexing program for all symmetries. *J. Appl. Crystallogr.* **1985,** *18*, 367-370.
2. Casella, I. G.; Di Fonzo, D. A., Anodic electrodeposition of cobalt oxides from an alkaline bath containing Co-gluconate complexes on glassy carbon. An electroanalytical investigation. *Electrochim. Acta* **2011,** *56*, 7536-7540.
3. Castro, E. B.; Gervasi, C. A.; Vilche, J. R., Oxygen evolution on electrodeposited cobalt oxides. *J. Appl. Electrochem.* **1998,** *28*, 835-841.
4. Sawyer, D. T.; Sobkowiak, A.; Roberts, J. L., *Electrochemistry for Chemists*. John Wiley & Sons New York, 1995.
5. Yang, J.; Cheng, H.; Frost, R. L., Synthesis and characterisation of cobalt hydroxy carbonate Co2CO3(OH)2 Nanomaterials. *Spectrochim. Acta, Part A* **2011,** *78*, 420-428.
6. Avramov, L.; Betschev, C., Derivatographische Untersuchungen an einem basischen Kobaltcarbonat. *Z. Anorg. Allg. Chem.* **1971,** *383*, 96-102.
7. Tronto, J.; Bordonal, A. C.; Naal, Z.; Valim, J. B., Conducting Polymers / Layered Double Hydroxides Intercalated Nanocomposites. In *Materials Science: Advanced Topics*, Mastai, Y., Ed. InTechOpen: 2013.
8. Richetta, M.; Digiamberardino, L.; Mattoccia, A.; Medaglia, P. G.; Montanari, R.; Pizzoferrato, R.; Scarpellini, D.; Varone, A.; Kaciulis, S.; Mezzi, A.; Soltani, P.; Orsini, A., Surface spectroscopy and structural analysis of nanostructured multifunctional (Zn, Al) layered double hydroxides. *Surf. Interface Anal.* **2016,** *48*, 514-518.
9. Hu, L.; Peng, Q.; Li, Y., Selective Synthesis of Co3O4 Nanocrystal with Different Shape and Crystal Plane Effect on Catalytic Property for Methane Combustion. *J. Am. Chem. Soc.* **2008,** *130*, 16136-16137.
10. Liu, X.; Prewitt, C. T., High-temperature X-ray diffraction study of Co3O4: Transition from normal to disordered spinel. *Phys. Chem. Miner.* **1990,** *17*, 168-172.
11. Howell, O. R.; Jackson, A., The change in the absorption spectrum of cobalt chloride in aqueous solution with increasing concentration of hydrochloric acid. *Proc. Roy. Soc. A* **1933,** *142*, 587-597.
12. Wen, T.; Qu, F.; Li, N. B.; Luo, H. Q., A facile, sensitive, and rapid spectrophotometric method for copper(II) ion detection in aqueous media using polyethyleneimine. *Arab. J. Chem.* **2017,** *10*, S1680-S1685.
13. Gunasekaran, S.; Anbalagan, G.; Pandi, S., Raman and infrared spectra of carbonates of calcite structure. *J. Raman Spectrosc.* **2006,** *37*, 892-899.
14. Hans, H. A.; Paul, F. K., Infrared ansorption frequency trends for anhydrous normal carbonates. *Am. Mineral.* **1963,** *48*, 124-137.
15. Kislenko, V. N.; Oliynyk, L. P., Complex formation of polyethyleneimine with copper(II), nickel(II), and cobalt(II). *J. Polym. Sci., Part A: Polym. Chem.* **2002,** *40*, 914-922.
16. Schenk, A. S.; Cantaert, B.; Kim, Y.-Y.; Li, Y.; Read, E. S.; Semsarilar, M.; Armes, S. P.; Meldrum, F. C., Systematic Study of the Effects of Polyamines on Calcium Carbonate Precipitation. *Chem. Mater.* **2014,** *26*, 2703-2711.
17. Sampanthar, J. T.; Zeng, H. C., Arresting Butterfly-Like Intermediate Nanocrystals of β-Co(OH)2 via Ethylenediamine-Mediated Synthesis. *J. Am. Chem. Soc.* **2002,** *124*, 6668-6675.
18. Kobayashi, S.; Hiroishi, K.; Tokunoh, M.; Saegusa, T., Chelating properties of linear and branched poly(ethylenimines). *Macromolecules* **1987,** *20*, 1496-1500.